Journal of Atmospheric and Solar-Terrestrial Physics xxx (2017) 1–10

Contents lists available at ScienceDirect

Journal of Atmospheric and Solar-Terrestrial Physics

journal homepage: www.elsevier.com/locate/jastp

NOAA POES and MetOp particle observations during the 17 March 2013 storm

Finn Søraas [a,*], Marit Irene Sandanger [a], Christine Smith-Johnsen [b]

[a] Birkeland Centre for Space Science, Department of Physics and Technology, University of Bergen, Allegaten 55, N5007 Bergen, Norway[1]
[b] Section for Meteorology and Oceanography, University of Oslo, Oslo, Norway

ARTICLE INFO

Keywords:
March 2013 storm
Particle precipitation
Isotropic boundary
Storm time equatorial belt

ABSTRACT

Five National Oceanic and Atmospheric Administration and Meteorological Operational polar orbiting low altitude satellites were in operation during the 17 March 2013 storm. They were equipped with identical instruments to measure the precipitation of energetic particles over a large energy range. Well calibrated particle data, gives the opportunity of complete ILAT/MLT plots on a time resolution of 3 h throughout the storm. During the storm sudden commencement and main phase of the storm, an isotropic proton precipitation occurred at almost all magnetic local time and the Isotropic Boundary (IB) coincided with the inner boundary of the Ring Current (RC) as determined by the Van Allen Probes. Thus the IB on the night/dusk sector is a measure of how deep the ring current develops in the inner magnetosphere. The electron and proton precipitation is closely connected with substorms and the convective electric field created by the solar wind. A loss cone totally filled with particles indicates the occurrence of particles injection into the RC, while a partly filled loss cone means that the RC particles experienced a loss.

The above 1 MeV electrons disappear in the storm main phase, but appears with increased intensity in the recovery phase. They are limited to the invariant latitude region 50° to 62°. The lower energy electrons penetrate deeper into the magnetosphere. During geomagnetic storms a Storm Time Equatorial Belt (STEB) of energetic neutral atoms and ions is found to exist at low altitudes around the geomagnetic equator. Their source is the RC protons existing at larger L-values. The STEB appears first in the midnight/evening sector and then later in the morning sector largely consistent with the drift of the RC ions and in accordance with results from ground based magnetic observations. During the main phase of the storm, the outer part of the RC will experience magnetopause shadowing and will be lost at the magnetopause. Maximum particle injection into the ring current is associated with the most rapid fall in Dst. The maximum STEB intensity is associated with minimum Dst and strongest RC.

1. Introduction

Low altitude polar orbiting satellites can monitor the energetic particle precipitation to the upper atmosphere with high temporal and spatial resolution. Such observations are essential for testing and imposing constraints on theoretical models for magnetospheric processes, observational facts which the models must account for. Over the years many statistical and event studies (Amundsen et al., 1972; Hultqvist et al., 1976; Sergeev et al., 1983) have shown that during the main phase of the storm, the loss cone is filled and the particle precipitation is isotropic.

The main precipitation mechanism for proton precipitation is considered to be the scattering in a magnetic field with a small curvature compared with the gyro radii of the protons (Sergeev et al., 1983). The protons can also be scattered into the loss cone in regions where they becomes unstable and generate Electromagnetic Ion Cyclotron (EMIC) waves for instance in the plasma pause region or in plumes (Yahnin and Yahnina, 2007). Electrons precipitate mostly by interaction with Chorus waves outside and Hiss inside the plasma sphere.

The injection of protons/ions and electrons into the inner magnetosphere give rise to the Earth's Ring Current (RC). The particles originate in the plasma sheet and are brought into the inner magnetosphere by the electric field created by the solar wind passing the Earth (Chen and Wolf, 1993). In addition to this, particles are also injected impulsively into the

* Corresponding author.
E-mail address: finn.soraas@uib.no (F. Søraas).
[1] URL: https://birkeland.uib.no/.

http://dx.doi.org/10.1016/j.jastp.2017.09.004
Received 3 May 2017; Received in revised form 10 August 2017; Accepted 4 September 2017
Available online xxxx

region by substorms and bursty bulk flow.

The injection of particles into the RC is closely connected with the particle precipitation into the night side auroral zone. The particles injected from the plasma-sheet have a pitch angle distribution that fills the atmospheric loss cone. This is the case during the main phase of the geomagnetic storm when the RC is building up. Thus the isotropic particle precipitation into the upper atmosphere is a proxy for the injection rate into the RC. Using the energy of the protons precipitating into the night side as the source population in the Burton relation (Burton et al., 1975) a RC-index was calculated (Søraas et al., 2002) that correlated highly with the pressure corrected Dst.

During the recovery phase of the storm the pitch angle distribution of the electrons and protons is anisotropic. These particles are weakly scattered by waves and represent a loss of particles from the RC (Jordanova et al., 1997). An important loss process for RC ions is charge exchange of energetic ions with the Earths geocorona giving rise to Energetic Neutral Atoms (ENA) (Tinsley, 1979). These ENA are unaffected by the Earths magnetic field and escape in all directions. During geomagnetic storms, ENA is detected at low altitudes around the geomagnetic equator. This radiation was called Storm Time Equatorial Belt (STEB) by (Søraas et al., 2003) and has been discussed in a number of papers (e.g. (Sørbø et al., 2006; Søraas and Sørbø, 2013)). The STEB ENA is created by the RC protons at an altitude of 2.5–6 Earth radii. These ENA enable us to track the RC both in intensity and MLT. Low altitude ENA emissions were first imaged by the Swedish ASTRID satellite (Brandt et al., 1997) and were extensively imaged by the Medium Energy Neutral Atom (MENA) and High Energy Neutral Atom (HENA) instruments on the IMAGE spacecraft during its 5.75-year mission.

The aim of this paper is to study the low altitude precipitation of energetic electrons and protons over a large energy range during a magnetic storm. While most studies have considered particles with energies below 20 keV (Newell et al., 1998), this study includes energies up to 10's and 100's of keV. The 17 March 2013 storm was selected because during that storm 5 POES (Polar Orbiting Environment Satellites) were in operation and could be related to observations by the Van Allen Probes in and near the equatorial plane. Several studies of the 17 March 2013 storm using observations from the Van Allen Probes in the equatorial region have been reported (e.g. (Lyons et al., 2016; Baker et al., 2014; Foster et al., 2014; Gkioulidou et al., 2014)). However, here observations around 800 km altitude are discussed. It is an advantage to study this at low altitudes where the loss cone is large near 90°, compared with the one in the equatorial plane which is only a few degrees wide.

2. Geophysical conditions

Fig. 1 gives an overview of the solar wind conditions during the 17 March 2013 storm. It is a coronal mass ejection-driven event with a shock that impacted the magnetosphere at 06:00 Universal Time (UT) (Baker et al., 2014). The shock is manifested by a Storm Sudden Commencement (SSC) seen in the Dst. The Bz goes negative at the shock and remain negative for approximately 18 h. It oscillates slightly and exhibits two minima going down to −15 nT and −12 nT, respectively. The storm reaches a minimum Dst of −140 nT and is most pronounced in the midnight to afternoon sector (00–18 Magnetic Local Time (MLT)) as seen in the SuperMAG Ring current (SMR) indices at the bottom panel of Fig. 1. During the storm recovery phase the RC field becomes more independent of MLT. After an initial fast recovery the storm enters into a long slow recovery phase.

3. Satellites and instrumentation

In March 2013, five satellites (POES 15, 16, 18 and 19 and METOP-2) were in operation. The satellites have identical instrumentation which is most valuable when comparing their observations. The National Oceanic and Atmospheric Administration (NOAA) POES and MetOp-02 satellites are Sun-synchronous low-altitude polar orbiting spacecraft. Their orbital

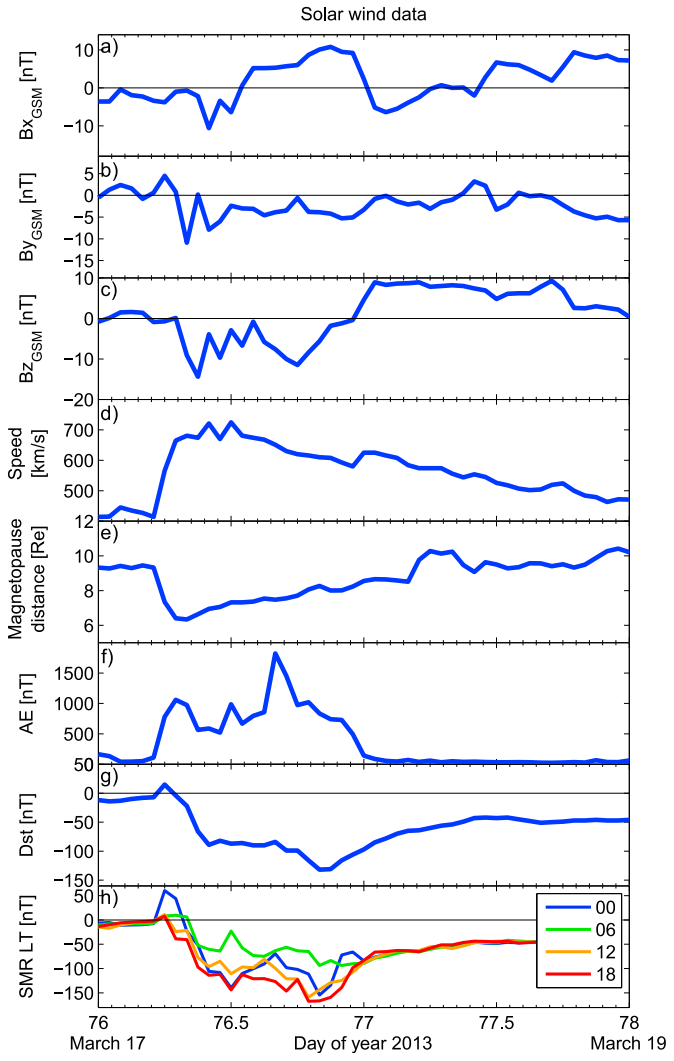

Fig. 1. The figure displays the solar wind data. Panel a)-c) exhibit the components of the interplanetary magnetic field, Bx, By and Bz, in Geocentric Solar Magnetospheric (GSM) coordinates. Panel d) shows the solar wind speed. Panel e) exhibits the calculated magnetopause distance in Re, based upon the solar wind speed and density. The AE index and Dst are displayed in panel f) and g). The SMR LT index (Gjerloev, 2012) is displayed in panel h) with blue line for 00 LT, green line for 06 LT, orange line for 12 LT, and red line for 18 LT. (For interpretation of the references to colour in this figure legend, the reader is referred to the web version of this article.)

period is about 103 min, resulting in 14–15 orbits each day. The footprint of the orbits are located at different MLT sectors, as visualized in Fig. 2. In the midnight sector the MLT coverage is good in the southern hemisphere while the noon sector has a good coverage in the northern hemisphere. The satellites are launched alternately in low-altitude (~825 km) morning orbits, and high-altitude (~865 km) afternoon orbits.

The MEPED (Medium Energy Proton Electron Detector) instrument consists of two identical proton and electron telescope, one viewing nearly radially outward from Earth and the other viewing nearly anti-parallel to the satellite velocity vector and normal to the vertical telescope; for details, see (Evans and Greer, 2004). These two telescopes will be referred to as the 0° and the 90° detectors. At high latitudes this is approximately the pitch angle of the particles being measured by the respective detectors. The detectors have an opening angle of 30° FWHM. In Fig. 3 the opening angles of the telescope is shown in relation to the atmospheric loss cone.

The MEPED instrument measures both protons and electrons, but can not distinguish between different ions. The electron detector has a nickel foil protecting it from protons below 135 keV. The proton detectors are

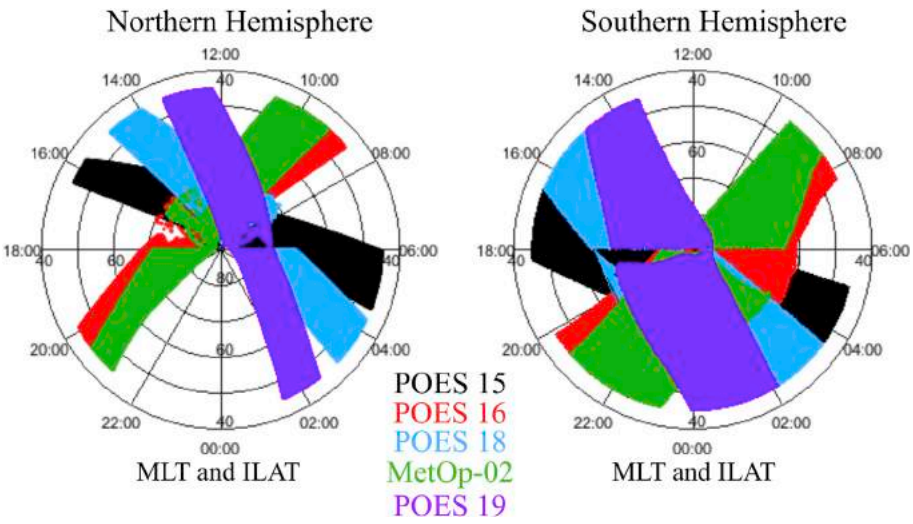

Fig. 2. The footprint of the different NOAA POES 15, 16, 18, 19 and MetOp-02 satellites in the Northern and Southern hemisphere during March 2013, plotted in ILAT versus MLT coordinates.

equipped with broom magnets excluding electrons with energies below around 1 MeV to be detected. Table 1 gives an overview of the nominal energy thresholds of the MEPED proton and electron detectors. The P6 energy channel can detect relativistic electrons when the P5 detector exhibits no counts (Yando et al., 2011), which means that no protons above 2.5 MeV are present. The relativistic electrons detected by the proton energy channel P6, are noted as a fourth electron integral channel, E4, in Table 1.

In addition to using data from the MEPED, data from TED (Total Energy Detector) will be used. The TED consist of two detectors, one at 0° and one at 30° degree with the vertical, each capable of measuring electrons and protons in the energy range 0.2–20 keV. The particle flux in five energy channels and the total energy input to the atmosphere below 20 keV are determined. In this study we only use the total energy input below 20 keV from the TED detector. This is given in Table 1 for completeness. As the 0° and 30° TED detectors show about the same time behaviour, only 0° detector is used in this study. For details about the MEPED and TED detectors, see (Evans and Greer, 2004).

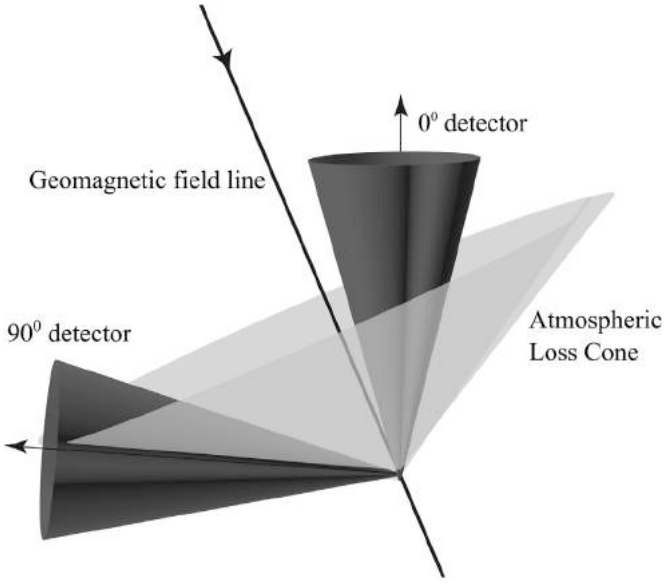

Fig. 3. The opening angle and direction of the 0° and the 90° detector is shown together with to the atmospheric loss cone at one specific latitude. The size of the atmospheric loss cone as well as the angle to the two detectors will vary throughout the orbit.

4. Observations

4.1. Time evolution of the proton precipitation

In Figs. 4 and 5 the intensity of the 0° and 90° protons are shown in color as Invariant Latitude (ILAT) versus UT for 01 and 14 MLT respectively. The 0° protons are shown in the left panel and the 90° in the right panel. The four top left panels exhibit protons in the energy bands (0.2–20), (30–80), (80–250) and (250–800) keV and the bottom panel the Dst index. In the right panels the 90° protons are shown in a similar manner. The top panel is empty because TED is not observing at 90°. These proton energies are typical for the ring current. Only data from POES 19 are shown as the other satellites observe similar particle behaviour. The observations cover the time from March 16 to March 22. It thus starts about a day before the storm commences. During that time, at MLT 01 (Fig. 4), there was some proton precipitation located around ILAT 70° and the Dst was slightly depressed due to a small dip in the Dst early on March 16. When the interplanetary shock hits the magnetosphere, with the subsequent SSC, there is an immediately poleward movement and increased intensity in all of the proton energy channels for both the 0° and 90° protons. During the main phase of the storm the precipitation in all channels increases and moves equatorward indicating that the ring current particles are injected deeper and deeper into the inner magnetosphere reaching down to L = 2.7. The precipitation is closely related to the time variation of the Dst (Søraas et al., 2002). The precipitation is most intense when the rate of change in Dst is largest, indicating maximum particle injection into the RC, that is in the beginning of the main phase.

In the right hand panel of Fig. 4 the flux of the 90° protons are shown. The overall behaviour of these particles are much the same as for the 0°, but they extend equator ward of the 0° protons indicating a partly filled

Table 1
Overview of the nominal energy channels of the TED and MEPED proton and electron detectors. These energies are valid for both the MEPED 0° and the 90° detector and the TED 0° and the 30° detector.

Channel	Proton energy [keV]	Channel	Electron energy [keV]
TED			
P total	<20	E total	<20
MEPED			
P1	30–80	E1	>30
P2	80–250	E2	>100
P3	250–800	E3	>300
P4	>6900	E4	>1000

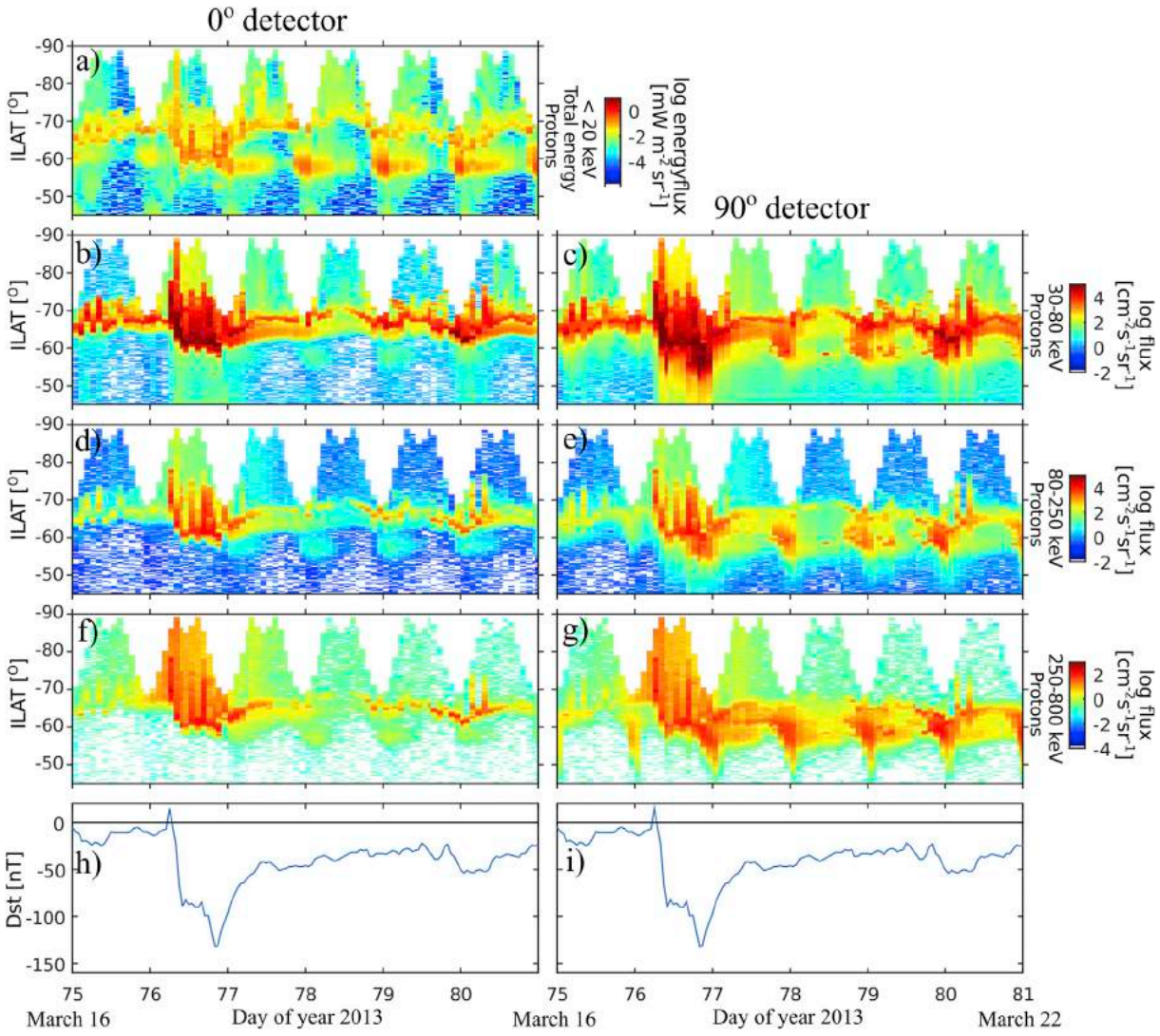

Fig. 4. The 7 color coded ILAT-UT plot exhibit logarithmic flux of protons measured by the 0° detector on the left side and the 90° detector on the right side. The data are from March 17th to 22th in 2013 measured by the POES 19 satellite during the Southern Hemisphere passes, around 01 MLT. Panel a) shows total energy protons <20 keV from the 0° TED detector, while the panels b)-k) show protons from the MEPED detector. The panels b)-k) show the following energy bands: b) and c) 30–80 keV, d) and e) 80–250 keV, f) and g) 250–800 keV. Notice that panel a), f), and g) have different color scale compared to the other panels. The Dst index is shown in the bottom panels h) and i).

loss cone and weak pitch angle scattering at these latitudes. When the storm starts to recover as seen in the Dst there is an abrupt decrease in the particle precipitation and the storm enters into the recovery phase. This phase is rapid for half a day and then develops into a long and slower phase. There is, however, a continuous precipitation of protons at high latitudes between 65° and 70° ILAT. This injection of protons maintain the RC at a low level shown by the Dst. (Sandanger et al., 2005) and (Søraas et al., 2004) have discussed this in relation to HILDCAA (High Intensity Long Duration Continuous AE Activity) storms. The proton precipitation exhibits a daily variation in intensity, particularly seen in the 90° protons. This is due to the Earth's weaker magnetic field at longitudes associated with the South Atlantic Anomaly. The daily modulation seen in the TED observations between ILAT 50° to 62°, upper left panel, is due to penetration of relativistic electrons.

In Fig. 5 the proton precipitation at MLT = 14 is shown. The black line in panel a), b) and c) shows the calculated projection of the magnetopause. The estimate of the magnetopause location is based on equilibrium between the dynamic ram pressure from the solar wind and the magnetic pressure from the Earths magnetic field, using the measured solar wind density and velocity. The precipitation at this MLT is less than at MLT = 01, both in intensity and latitudinal extent.

Assuming that the protons are injected from the plasma sheet on the night side they drift westward to reach 14 MLT. During the main phase they exhibit a narrow band of isotropic precipitation. Except for a poleward expansion during the shock, SSC, the dayside precipitation occur below ILAT 70°. It seems to be equator ward of the projection of the magnetopause boundary. The particles on drift orbits above ILAT 70° will encounter the magnetopause. Thus no protons from the night side can reach above this latitude on the dayside.

Poleward of the main precipitation zone, the auroral oval, a band of precipitation can be seen around 75° ILAT. This is cusp precipitation, clearly seen in the below 20 keV protons, but also evident in the energy band (30–80) keV. The cusp precipitation exhibits a daily variation in ILAT caused by the satellite sampling at different MLT during the day. During the recovery phase, very little precipitation is seen in the 0° detector while the 90° detector flux indicates weak pitch angle scattering in the equator ward region.

During the main phase of the storm the protons in the <20 keV and 30–80 keV channels precipitate poleward of this boundary. If the magnetopause terminated the particle drift orbits, no drifting particles from the nightside should be seen poleward of this projected magnetopause. One explanation for this finding could be that the convection field,

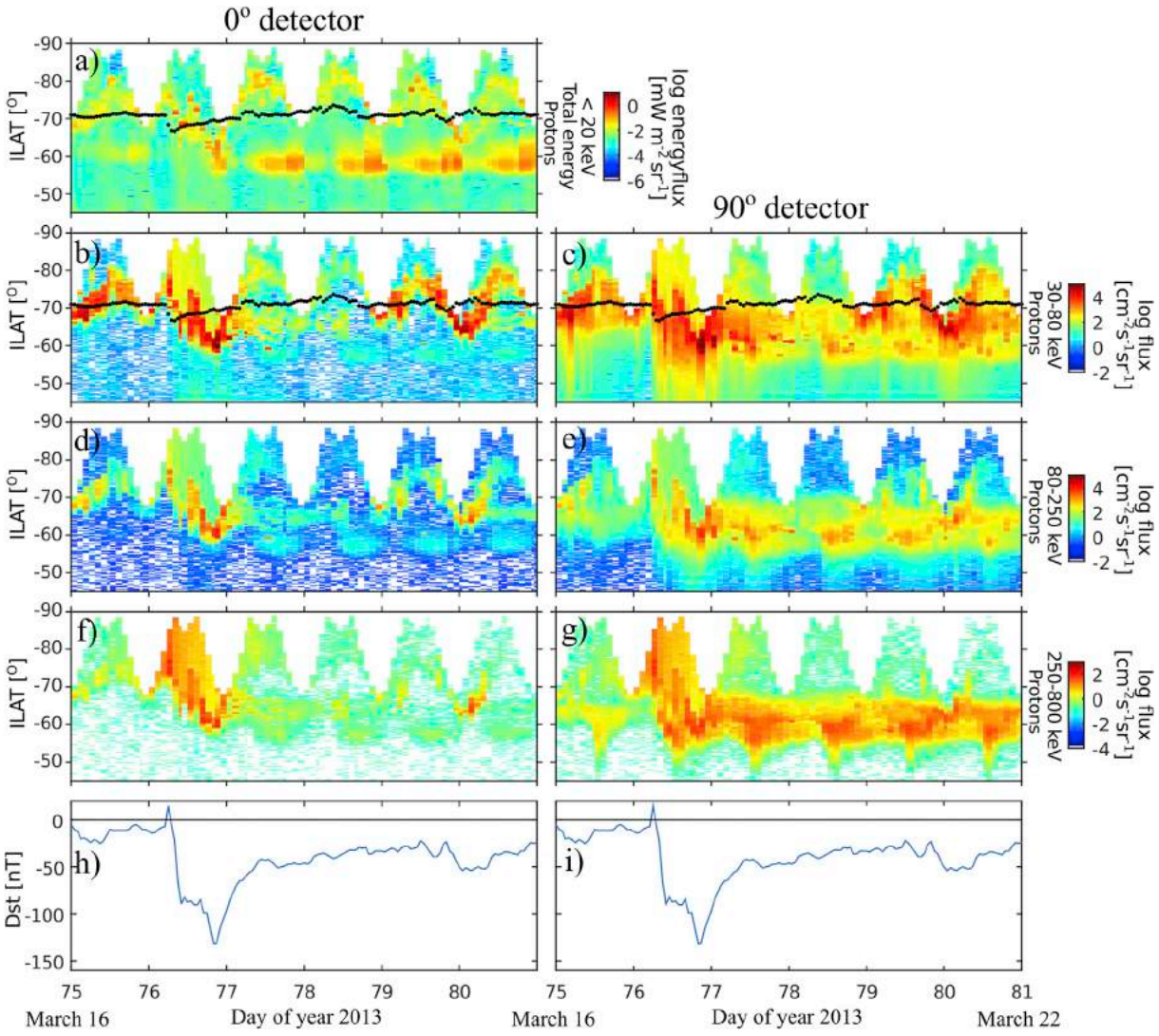

Fig. 5. The 7 color coded ILAT-UT plot exhibit logarithmic flux of protons measured by the 0° detector on the left side and the 90° detector on the right side. The data are from March 17th to 22th in 2013 measured by the POES 19 satellite during the Southern Hemisphere passes, around 14 MLT. Panel a) shows total energy protons <20 keV from the 0° TED detector, while the panels b)-k) show protons from the MEPED detector. The panels b)-k) show the following energy bands: b) and c) 30–80 keV, d) and e) 80–250 keV, f) and g) 250–800 keV. Notice that panel a), f), and g) have different color scale compared to the other panels. The calculated projection of the magnetopause position is marked with a black line in panel a), b) and c). The Dst index is shown in the bottom panels h) and i).

convects the particles poleward as they stream towards the ionosphere. When the particles stream towards the Earth, they are at the same time convected poleward at the ExB/B^2 speed. Particles with low velocity will be transported further poleward. (Søraas et al., 1980) used this effect to explain particle velocity dispersion in and near the cusp. The observations of the >30 keV protons in the cusp could be related to the Cusp Energetic Particles described by (Chen et al., 1998).

4.2. Time evolution of the electron precipitation

In Figs. 6 and 7 the intensity of the 90° and 0° electrons are shown in color as a function of ILAT and UT. The 0° electrons are shown in the left panel and the 90° in the right panel. The panels from the second to the fifth rows show the energy bands (>30), (>100), (>300) and (>1000) keV and the bottom panel the Dst index. The top panel exhibits the energy flux of electrons below 20 keV.

In the right panels the 90° electrons are shown in a similar manner with the top panel empty because TED does not measure at 90°. The plots cover the same time interval as the proton observations. During March 16, the day before the storm, there are some precipitation in the <20 keV and in the >30 keV channels. In the 90° detector the slot region is seen in the >30 and > 100 keV channels.

When the interplanetary shock hits the magnetosphere, with it's subsequent SSC, there is an immediately pole ward movement and increased intensity in the three lowest MEPED channels, that is energies up to above 300 keV. The <20 keV electrons also exhibit a large increase in intensity and spatial extent. Then during the main phase of the storm the precipitation in all three channels move equator ward. During the recovery phase of the storm the 0° degree electrons fade away and are only shown in a limited ILAT band around 65°. The 90° electrons exhibits a much higher intensity. They also commence at the shock arrival with a poleward expansion, and then they move equator ward during the main phase of the storm. The slot region is closed in.

The right fifth panel displays relativistic electrons at 90° with energies above 1 MeV. They are limited in the ILAT band 50° to 62°. They exhibit a decrease during the storm main phase and a gradual build up during the storm recovery phase as have been discussed by (Reeves, 1998; Sandanger et al., 2009) and others. The relativistic electrons penetrate somewhat below L = 3. This is in accordance with observations by (Baker et al., 2016), that there seems to be an impenetrable boundary for the

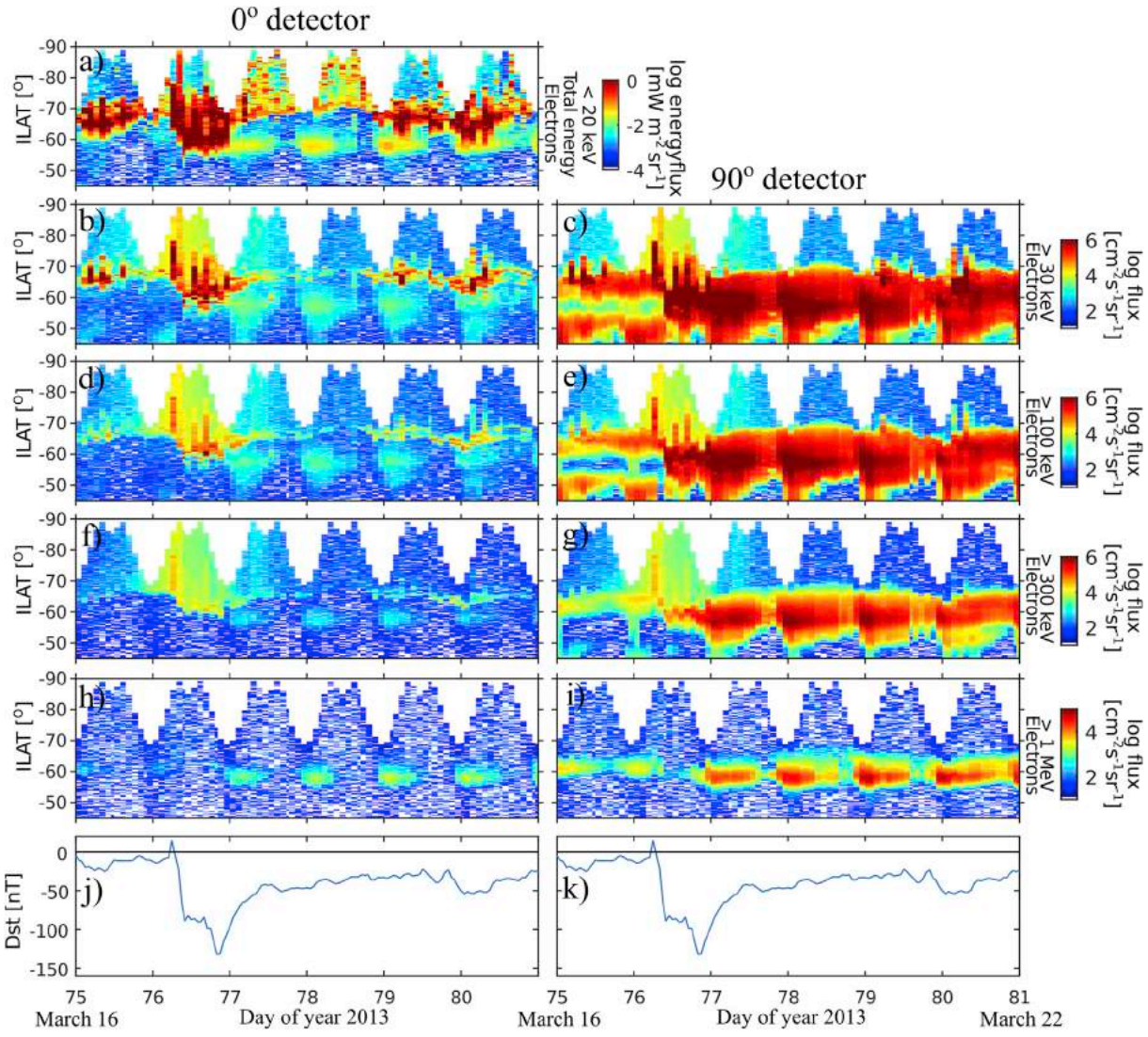

Fig. 6. Data from the 0° (left side) and 90° (right side) electrons are shown in color coded logarithmic flux as ILAT versus UT, from March 17th to 22th in 2013. The data are from POES 19 during Southern Hemisphere passes around 01 MLT. Panel a) shows total energy electrons <20 keV from the 0° TED detector, while the panels b)-i) show electrons from the MEPED detector. The panels b)-i) show the following integral energies: b) and c) > 30 keV, d) and e) > 100 keV, f) and g) > 300 keV, h) and i) > 1000 keV. The latter integral energy are contaminated electrons measured by the MEPED P6 channel. Notice that panel a), h), and i) have different color scale compared to the other panels. The Dst index is shown in the bottom panels j) and k).

>1 MeV electrons. The lower energy electrons are well inside this L-value. The relativistic electrons at 0° is exhibited at the left fifth panel. They exhibit a very low intensity, indicating a very low scattering of relativistic electrons into the loss cone. Both the 0° and particularly 90° protons and electrons exhibit a daily modulation due to changes in the Earths magnetic field versus geographic longitude, due to the weaker magnetic field associated with the South Atlantic Anomaly.

4.3. Method of deriving MLT/ILAT polar plot

The five NOAA POES and MetOp satellites, that were in operation in March 2013, have different ages, ranging from 4 years to 15 years of operational time. The expected lifetime of the satellites are 3 years, but the long-lived satellites give us new information as they are measuring at different MLT sectors as the MLT change over time, and complement each other. The harsh environment over time, however, degrade the detectors, and work has been done in order to derive correction factors (Asikainen and Mursula, 2011; Sandanger et al., 2015; Ødegaard et al., 2016).

In Section 4.4, the particle precipitation from all 5 satellites are used in combination to get a MLT/ILAT overview. The proton data are corrected due to detector degradation, as the uncorrected proton data will give rise to a systematic error with lower fluxes at MLT sectors where the oldest spacecraft are measuring. In Fig. 8 the method for establishing these interpolated multi satellite plots is illustrated. Panel a) shows the orbits from the 5 satellites during a 3 UT hours timespan. The orbits are interpolated both forward (in the satellite orbital direction) and backward. Panel b) shows how the data are sorted into bins of 4° in latitude and 10° in longitude. Panel c) shows the result after the interpolation in the longitudinal direction between all the satellites. The resulting matrix is transformed from geographic longitude to MLT coordinates.

4.4. Evolution of the particle precipitation in MLT/ILAT polar plot

Fig. 9 displays interpolated multi satellite polar plots from the Southern Hemisphere during the March storm. The upper panels show 30–80 keV proton flux from the 90° detector, while flux from the 0° detector is exhibited in the middle panels. The polar plots refer to six times during the storm. Panel (i) displays the time immediately before the storm and exhibits a small and contracted auroral oval. Panel (ii) refers to the time around the SSC. It exhibits a great extended oval with intense

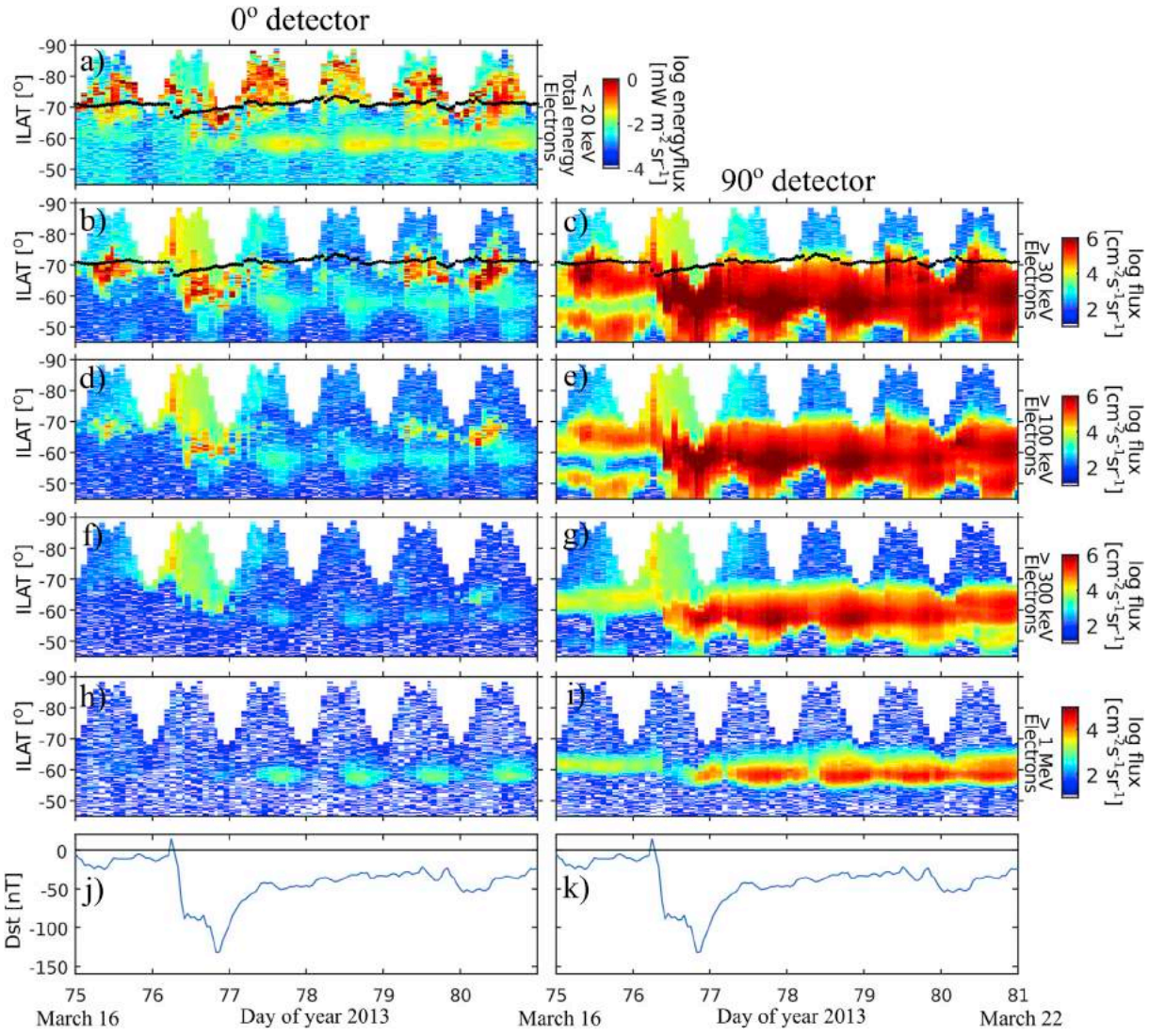

Fig. 7. Data from the 0° (left side) and 90° (right side) electrons are shown in color coded logarithmic flux as ILAT vs. UT, from March 17th to 22th in 2013. The data are from POES 19 during Southern Hemisphere passes around 14 MLT. Panel a) shows total energy electrons <20 keV from the 0° TED detector, while the panels b)-i) show electrons from the MEPED detector. The panels b)-i) show the following integral energies: b) and c) > 30 keV, d) and e) > 100 keV, f) and g) > 300 keV, h) and i) > 1000 keV. The calculated projection of the magnetopause position is marked with a black line in panel a), b) and c). The latter integral energy are contaminated electrons measured by the MEPED P6 channel. Notice that panel a), h), and i) have different color scale compared to the other panels. The Dst index is shown in the bottom panels j) and k).

proton precipitation in the nightside afternoon sector. The rest of the panels show how the precipitation changes throughout the storm. The two panels on the bottom exhibit the Dst and the AE index. The times for the different polar plots are marked by vertical lines. The proton penetration boundary found by the Van Allen Probes during the March storm (see Fig. 10 of (Lyons et al., 2016), are marked as white points with blue borderlines in the 8 polar-view-plots that have matching UT time with the Van Allen Probe findings. These white markers in Fig. 9 show how the isotropic boundary are coincident with the inner boundary of the ring current as determined by the Van Allen Probes in the equatorial region.

4.5. ENA from the ring current

With multiple satellites at different MLTs in operation during the storm it is possible to get good observations of the STEB and thus to some degree the time evolution of the ring current. In Fig. 10 the ENA observations at the geomagnetic equator for four of the satellites (POES 15, 16, 18, 19) are presented. The STEB intensity is observed by each satellite at two MLTs 12 h apart. It is seen that during the early main phase of the storm there is a difference in the intensity at the two MLTs. The ENA on the night side appear before the day side ENA observation. This reflects the drift of the ring current protons towards west from their injection at the night side. During the storm recovery phase the observations at the two MLTs approach each others indicating that the RC becomes symmetric. The intensity is independent of MLT. The fact that the same satellite measures the same intensity 12 MLT hours apart indicates that the RC has become symmetric. One can also notice that the newer satellites POES 19 and 18 show more or less the same intensity during the recovery phase. POES 15 and 16 exhibits a much lower intensity than the others, due to the previously mentioned radiation damage which reduce the sensitivity and increase the energy levels. Fig. 10a)–d) exhibit particles with nominal energy >30 keV, but the enhanced energy levels due to degradation in March 2013 (Sandanger et al., 2015; Ødegaard et al., 2016; Ødegaard, 2016), are marked in these four panels.

The decay of the STEB during the recovery phase is due to charge exchange. Most of the ENA production occur at the inner edge of the ring current where the geocorona is most dense. From simultaneous Van Allen Probe observations the inner edge of the ring current during the main phase of the storm coincident with the isotropic boundary (IB).

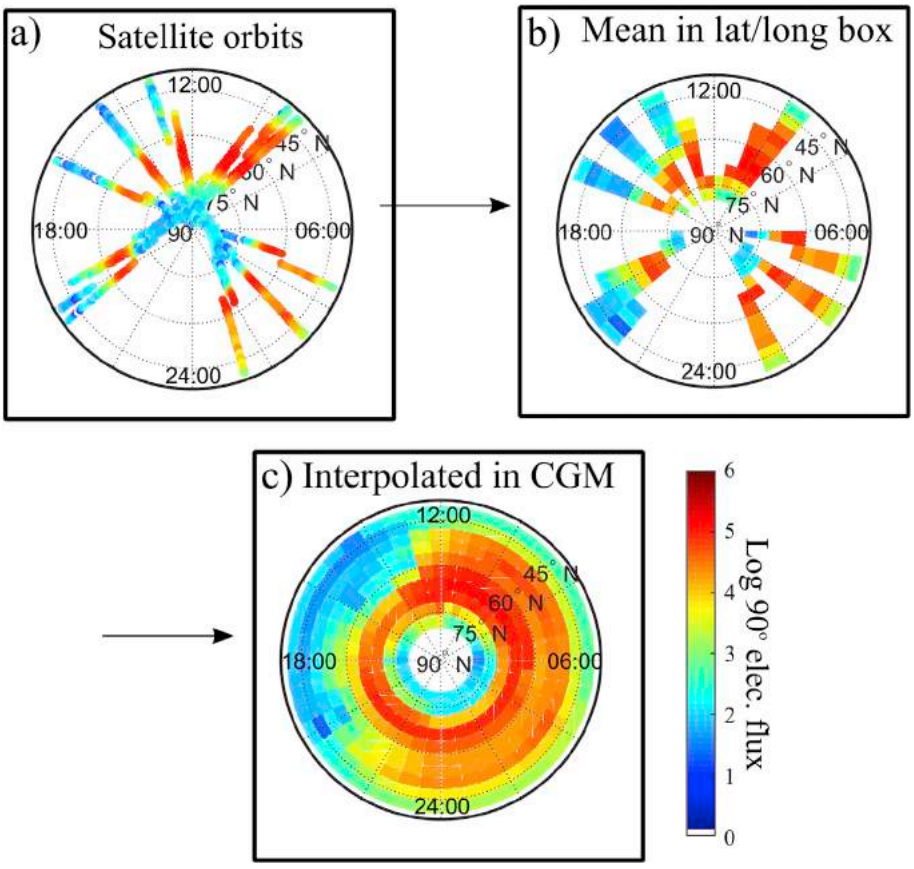

Fig. 8. Illustrates the method used to obtain the polar-view-plot in Fig. 9. Panel a) displays the orbits from POES 15, POES 16, POES 18, MetOp-02 and POES 19 during a 3 h UT time span. The orbits are interpolated in orbital direction first. Panel b) show how the data are sorted in 4° latitudinal and 10° longitudinal (or 40 min MLT) boxes. Panel c) shows the result after interpolating in the CGM-latitude direction.

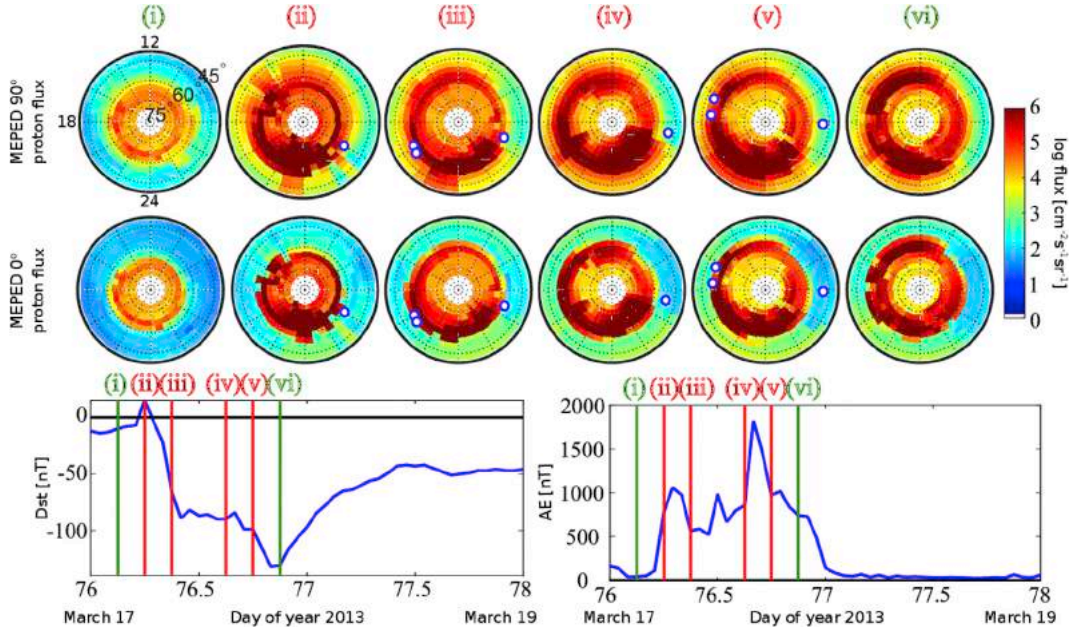

Fig. 9. The Figure displays twelve interpolated multi satellite plots from POES 15, POES 16, POES 18, MetOp-02 and POES 19 from the Southern Hemisphere during the March 2013 storm. The color coded MLT/ILAT plots shows 30–80 keV proton flux from the 90° detector (upper panels) and from the 0° detector (lower panels). The two panels at the bottom exhibit the Dst and AE indices. The four red and two green vertical lines in these panels, mark the time of the color coded multi satellite plots. The white points with blue borderlines in the plot marked with time (ii)-(v) illustrate the proton injection boundary found by Lyons et al., (2016).

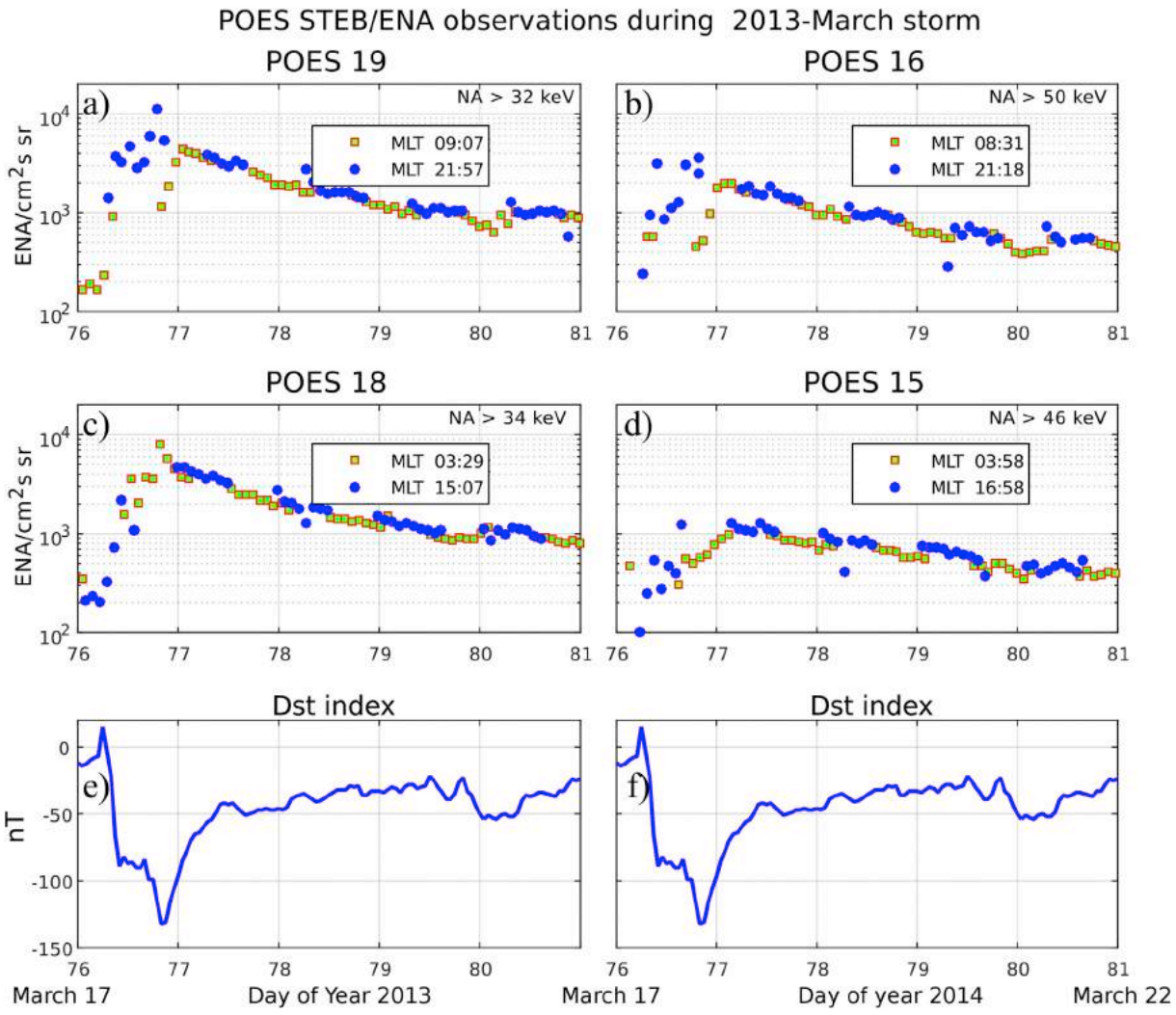

Fig. 10. The ENA observations from POES 19, POES 16, POES 18, and POES 15 are shown in panels a)-d). The measurements are sorted into either green squares or blue circles depending on the MLT sector. Panel e) and f) exhibit the Dst index. (For interpretation of the references to colour in this figure legend, the reader is referred to the web version of this article.)

5. Summary and conclusion

Observations from multiple NOAA POES and MetOp polar orbiting satellites for the 17 March 2013 storm have been presented. When the shock hits the magnetosphere, there is a rapid pole ward expansion to ILAT to about 75° for both electrons and protons. Immediately after the Bz goes negative, the particles penetrate deep into the magnetosphere down to L = 2.7 on the night side. Simultaneous observations of the inner edge of the RC by the Van Allen Probes confirm that this edge coincides with the IB. During the main phase of the storm they coincide at all MLTs, but during the storm recovery phase they only match on the night/dusk side where the plasma sheet particles are injected. By using well calibrated particle data from 5 satellites, gives us complete ILAT/MLT plots on a time resolution of 3 h throughout the storm. A selection of these ILAT/MLT plots are shown in Fig. 9.

Around the equator, ENAs from the RC are observed. They show that the RC is highly asymmetric during this initial phase and becomes symmetric during the recovery phase. This development agrees with the drift of the RC protons toward west, and with ground observations. Our observations can now be used to test and improve constraints for models of magnetospheric processes.

Acknowledgements

This study was supported by the Research Council of Norway under contract 223252. The authors thank the NOAA's National Geophysical Data Center (NGDS) for providing NOAA POES data. The OMNI data were obtained from the GSFC/SPDF OMNIWeb interface at http://omniweb.gsfc.nasa.gov. The authors thank the reviewers for good suggestions that have improved the paper.

References

Amundsen, R., Søraas, F., Lindalen, H., Aarsnes, K., 1972. Pitch-angle distributions of 100 to 300 kev protons measured by the Esro IB satellite. J. Geophys. Res. Space Phys. 77, 556–566. http://dx.doi.org/10.1029/JA077i004p00556.

Asikainen, T., Mursula, K., 2011. Recalibration of NOAA/MEPED energetic proton measurements. J. Atmos. Sol. Terr. Phys. 73, 335–347. http://dx.doi.org/10.1016/j.jastp.2009.12.011.

Baker, D., Jaynes, A., Li, X., Henderson, M., Kanekal, S., Reeves, G., Spence, H., Claudepierre, S., Fennell, J., Hudson, M., Thorne, R., Foster, J., Erickson, P., Malaspina, D., Wygant, J., Boyd, A., Kletzing, C., Drozdov, A., Shprits, Y., 2014. Gradual diffusion and punctuated phase space density enhancements of highly relativistic electrons: Van Allen Probes observations. Geophys. Res. Lett. 41, 1351–1358. http://dx.doi.org/10.1002/2013GL058942.

Baker, D., Jaynes, A., Kanekal, S., Foster, J., Erickson, P., Fennell, J., Blake, J., Zhao, H., Li, X., Elkington, S., Henderson, M., Reeves, G., Spence, H., Kletzing, C., Wygant, J., 2016. Highly relativistic radiation belt electron acceleration, transport, and loss: large solar storm events of March and June 2015. J. Geophys. Res. Space Phys. 121 (7), 6647–6660.

Brandt, P., Barabash, S., Norberg, O., Lundin, R., Roelof, E., Chase, C., Mauk, H., Thomsen, M., 1997. ENA imaging from the Swedish micro satellite Astrid during the magnetic storm of 8 February 1995. Adv. Space Res. 20 (4/5), 1061–1066. http://dx.doi.org/10.1016/S0273-1177(97)00561-9.

Burton, R., McPherron, R., Russel, C., 1975. An empirical relationship between interplanetary conditions and Dst. J. Geophys. Res. 80 (31), 4204–4214. http://dx.doi.org/10.1029/JA080i031p04204.

Chen, C., Wolf, R., 1993. Interpretation of high-speed flows in the plasma sheet. J. Geophys. Res. Space Phys. 98 (A12) http://dx.doi.org/10.1029/93JA02080, 21,409–21,419.

Chen, J., Fritz, T., Sheldon, R., Spence, H., Spjeldvik, W., Fennell, J., Livi, S., Russell, C., Pickett, J., Gurnett, D., 1998. Cusp energetic particle events: implications for a major acceleration region of the magnetosphere. J. Geophys. Res. Space Phys. 103 (A1), 69–78.

Evans, D., Greer, M., 2004. Polar Orbiting Environmental Satellite Space Environment Monitor-2: Instrument Descriptions and Archive Data Documentation, Technical Memorandum 93, NOAA, Boulder, Colorado OAR SEC 93, Version 1.4. January.

Foster, J., Erickson, P., Baker, D., Claudepierre, S., Kletzing, C., Kurth, W., Reeves, G., Thaller, S., Spence, H., Shprits, Y., Wygant, J., 2014. Prompt energization of relativistic and highly relativistic electrons during a substorm interval: Van Allen Probes observations. Geophys. Res. Lett. 41, 20–25. http://dx.doi.org/10.1002/2013GL058438.

Gjerloev, J., 2012. The supermag data processing technique. J. Geophys. Res. Space Phys. 117 (A9), 1–19. http://dx.doi.org/10.1029/2012JA017683.

Gkioulidou, M., Ukhorskiy, A., Mitchell, D., Sotirelis, T., Mauk, B., Lanzerotti, L., 2014. The role of small-scale ion injections in the buildup of earth's ring current pressure: Van Allen Probes observations of the 17 March 2013 storm. J. Geophys. Res. Space Phys. 119 http://dx.doi.org/10.1002/2014JA020096, 7,327–7,342.

Hultqvist, B., Riedler, W., Borg, H., 1976. Ring current protons in the upper atmosphere within the plasmasphere. Planet. Space. Sci. 24 (8), 783–797. http://dx.doi.org/10.1016/0032-0633(76)90115-X.

Jordanova, V., Kozyra, J., Nagy, A., Khazanov, G., 1997. Kinetic model of the ring current-atmosphere interactions. J. Geophys. Res. 102 (A7) http://dx.doi.org/10.1029/96JA03699, 14,279–14,291.

Lyons, L., Gallardo-Lacourt, B., Zou, S., Weygand, J.M., Nishimura, Y., Li, W., Gkioulidou, M., Angelopoulos, V., Donovan, E.F., Ruohoniemi, J.M., Anderson, B.J., Shepherd, S.G., Nishitani, N., 2016. The 17 march 2013 storm: synergy of observations related to electric field modes and their ionospheric and magnetospheric effects. J. Geophys. Res. Space Phys. 121 http://dx.doi.org/10.1002/2016JA023237, 10,880–10,897.

Newell, P., Sergeev, V., Bikkuzina, G., Wing, S., 1998. Characterizing the state of the magnetosphere: testing the ion precipitation maxima latitude (b2i) and the ion isotropy boundary. J. Geophys. Res. 103 (A3), 4739–4745. http://dx.doi.org/10.1029/97JA03622.

Ødegaard, June 2016. Energetic Particle Precipitation into the Middle Atmosphere - Optimization and Application of the NOAA POES MEPED Data. Ph.D. thesis. University of Bergen, Allegaten, 55, 5007 N-Bergen, Norway.

Ødegaard, L.-K., Tyssøy, H.N., Sandanger, M., Stadsnes, J., Søraas, F., 2016. Space weather inpact on the degradation of NOAA POES MEPED proton detectors. J. Space Weather Space Clim. 6 (A26), 1–15. http://dx.doi.org/10.1051/swsc/2016020.

Reeves, G., 1998. Relativistic electrons and magnetic storms: 1992-1995. Geophys. Res. Lett. 25 (11), 1817–1820. http://dx.doi.org/10.1029/98GL01398.

Sandanger, M., Søraas, F., Aarsnes, K., Oksavik, K., Evans, D., Greer, M., 2005. The Inner Magnetosphere: Physics and Modeling, Vol. 155 of Geophysical Monograph Series. AGU, Washington, DC, pp. 249–255. http://dx.doi.org/10.1029/155GM26. Ch. Proton injections into the ring current associated with Bz variations during HILDCAA events.

Sandanger, M., Søraas, F., Sørbø, M., Aarsnes, K., Oksavik, K., Evans, D., 2009. Relativistic electron losses related to EMIC waves during CIR and CME storms. J. Atmos. Sol. Terr. Phys. 71, 1126–1144. http://dx.doi.org/10.1016/j.jastp.2008.07.006.

Sandanger, M., Ødegaard, L.-K., Tyssøy, H.N., Stadsnes, J., Søraas, F., Oksavik, K., Aarsnes, K., 2015. In-flight calibration of NOAA POES proton detectors derivation of the MEPED correction factors. J. Geophys. Res. Space Phys. 120, 1–16. http://dx.doi.org/10.1002/2015JA021388.

Sergeev, V., Sazhina, E., Tsyganenko, N., Lundblad, J., Søraas, F., 1983. Pitch-angle scattering of energetic protons in the magnetotail current sheet as the dominant source of their isotropic precipitation into the nightside ionosphere. Planet. Space. Sci. 31 (10), 1147–1155.

Søraas, F., Sørbø, M., 2013. Low altitude observations of ENA from the ring current and from the proton oval. J. Atmos. Sol. Terr. Phys. 99, 104–110. http://dx.doi.org/10.1016/j.jastp.2012.10.003.

Søraas, F., Gustafsson, G., Borg, H., 1980. Field line topology in the dayside cusp region inferred from low altitude particle observations. Planet. Space. Sci. 28, 525–533.

Søraas, F., Aarsnes, K., Oksavik, K., Evans, D., 2002. Ring current intensity estimated from low-altitude proton observations. J. Geophys. Res. 107 (A7), 1149. http://dx.doi.org/10.1029/2001JA000123.

Søraas, F., Oksavik, K., Aarsnes, K., Evans, D., Greer, M., 2003. Storm time equatorial belt-an 'image' of ring current behaviour. Geophys. Res. Lett. 30 (2), 1052–1055. http://dx.doi.org/10.1029/2002GL015636.

Søraas, F., Aarsnes, K., Oksavik, K., Sandanger, M., Evans, D., Greer, M., 2004. Evidence for particle injection as the cause of Dst reduction during HILDCAA events. J. Atmos. Sol. Terr. Phys. 66, 177–186. http://dx.doi.org/10.1016/j.jastp.2003.05.001.

Sørbø, M., Søraas, F., Aarsnes, K., Oksavik, K., Evans, D., 2006. Latitude distribution of vertically precipitating energetic neutral atoms observed at low altitudes. Geophys. Res. Lett. 33 (L06108), 1–4. http://dx.doi.org/10.1029/2005GL025240.

Tinsley, B., 1979. Energetic neutral atom precipitation during magnetic storms: optical emission, ionization, and energy deposition at low and middle latitudes. J. Geophys. Res. 84 (A5), 1855–1863. http://dx.doi.org/10.1029/JA084iA05p01855.

Yahnin, A.G., Yahnina, T.A., 2007. Energetic proton precipitation related to ion-cyclotron waves. J. Atmos. Sol. Terr. Phys. 69, 1690–1706. http://dx.doi.org/10.1016/j.jastp.2007.02.010.

Yando, K., Millan, R., Green, J., Evans, D.S., 2011. A monte carlo simulation of the NOAA POES Medium energy proton and electron detector instrument. J. Geophys. Res. 116 (A10231), 1–13. http://dx.doi.org/10.1029/2011JA016671.